Available online at www.sciencedirect.com

SciVerse ScienceDirect

Journal of the European Ceramic Society 32 (2012) 1213–1220

www.elsevier.com/locate/jeurceramsoc

Load-bearing increase in alumina evoked by introduction of a functional glass gradient

Erik Dorthé, Yu Zhang *

Department of Biomaterials and Biomimetics, New York University College of Dentistry, 345 East 24th Street, New York, NY 10010, United States

Received 5 May 2011; received in revised form 24 October 2011; accepted 28 November 2011
Available online 20 December 2011

Abstract

Alumina is the most commonly used ceramic in orthopedics due mainly to its wear resistance and chemical inertness. However, alumina has relatively low load-bearing capacity compared to other advanced ceramics, such as zirconia. We hypothesized that grading the elastic modulus at the surfaces may substantially increase the load-bearing capacity of alumina. In this study, graded structures were fabricated by infiltrating glass into dense alumina plates, resulting in a diminished modulus at the surface layers. The plates were then bonded to polycarbonate substrates and subjected to flexural loading with various loading rates spanning five orders of magnitude (dynamic fatigue) in water. Infiltrated specimens showed an increase in flexural load over homogenous controls for all loading rates, despite the graded alumina exhibiting greater load rate dependence than their homogenous counterparts. Our results indicate that controlled elastic gradients at the surface could be highly beneficial in improving the load-bearing capacity of alumina ceramics.

Keywords: Al_2O_3; Glass ceramics; Fatigue; Strength; Biomedical applications

1. Introduction

Material selection for modern medical implants and dental prostheses has become a significant field of study. Ceramic materials have been chosen for load bearing applications due to their wear resistance and relative passivity in physiological environments. These positive traits are tempered by their inferior toughness and the undesirable flaw population created during ceramic processing and handling. Thus, ceramic materials, such as alumina and glass-ceramics, exhibit relatively poor flexural strength, especially when exposed to fatigue loading in wet environments.[1–3]

Composite ceramics have been designed in an attempt to improve strength and toughness while expanding functionality. Simple laminate materials have been developed for many years, in which a number of materials with different properties are bonded into a layered structure.[4] Though these composites do combine varying properties, the abrupt interface between the two materials often holds residual stresses[5,6] and sometimes delaminate under load.[7] These composites can be seen as the precursor to recent studies of functional gradients, and modeling and testing of such materials.

A material can be said to be functionally graded if it has two distinct values of an engineering property, with a gradual range of intermediary properties along the space between.[8] A variety of natural gradients occur, including a graded elastic modulus in hard tissues such as the human dentin and dentin–enamel junction.[5,9] Many engineered materials are graded in some manner, but a functionally graded material (FGM) is often characterized by a gradient purposefully formed using compositional or microstructural design.

Suresh, Jitcharoen and co-workers investigated the effects of increasing elasticity as a function of depth from the surface on the resistance to contact damage.[10,11] Aluminosilicate and oxynitride glasses were infiltrated into dense alumina and Si_3N_4 matrix, respectively, to create the elastic modulus gradient at the surface, which showed marked resistance to blunt indentation induced cone cracking otherwise seen in their

* Corresponding author at: Department of Biomaterials & Biomimetics, New York University College of Dentistry, Arnold and Marie Schwartz Hall of Dental Sciences, 345 East 24th Street, Rm 813C, New York, NY 10010, USA. Tel.: +1 212 998 9637; fax: +1 212 995 4244.
E-mail address: yz21@nyu.edu (Y. Zhang).

0955-2219/$ – see front matter © 2011 Elsevier Ltd. All rights reserved.
doi:10.1016/j.jeurceramsoc.2011.11.041

homogenous alumina and Si_3N_4 counterparts. This was hypothesized as being due to shifting of maximum stress from the contact surface into the material interior due to the modulus gradient.

We apply the concept of stress dissipation via elastic gradient to improve the much needed flexural fracture resistance of ceramics. Success has been shown in creating FG zirconia,[12–14] but use of zirconia in medical applications is debated because of potential hydrothermal instability of yttria stabilized zirconia (Y-TZP).[15–20] An FG alumina would have increased fracture resistance while retaining its phase stability.

In this study, we infiltrate the top and bottom surfaces of a relatively fine grained, medical grade alumina with a silica-based glass of similar coefficient of thermal expansion (CTE). This way a graded glass–alumina layer is introduced to the alumina surfaces without significant residual thermal stresses. Flexural resistance of graded alumina and homogeneous alumina are investigated using Hertzian contact flexural tests on flat-layer ceramic bonded to compliant substrate. Critical loads to produce flexural radial cracking at the ceramic lower surfaces are measured as a function of loading rates—dynamic fatigue. Data are analyzed using a slow-crack-growth (SCG) model; crack velocity exponents for both graded and homogeneous alumina are determined. Weibull analysis is conducted on normalized critical load. Theory behind improved fracture resistance by introduction of surface elastic grading is discussed.

2. Materials and methods

2.1. Sample preparation

The base ceramic used in this study was a commercial medical grade alumina (99.6% purity, density ~3.9 g/cm^3) (AD-996, CoorsTek, Golden, CO). Specimens were obtained in a plate form (2 mm thick, 23 mm in diameter); both top and bottom surfaces of the alumina plates were polished with successive grits to 0.5 μm finish. The final thickness of these plates was reduced to 1.5 mm ± 0.01 mm, measured with a digital caliper (Mitutoyo, Kawasaki, Japan). The average grain size of this alumina was measured as ASTM Grain Size Number 14, corresponding to approximately 2.8 μm, using a linear intercept method.[21]

Some of the polished plates were infiltrated with a silicate glass at both top and bottom surfaces, producing a glass/alumina/glass graded structure. The main composition of the infiltrating glass (>1 wt%), according to X-ray fluorescence (XRF) measurements, is: SiO_2 (71.60%), Al_2O_3 (10.55%), K_2O (8.00%), Na_2O (6.89%), and CaO (1.34%). The glass was formulated to create a CTE of $8.2 \times 10^{-6}\,^{\circ}C^{-1}$ (between 25 and 450 °C), which is identical to that of alumina. The particle size of the infiltrating glass ranged from 10 to 60 μm.

Specimens were coated on both surfaces with glass slurry created by suspending powdered glass in double deionized water and glass infiltration was conducted in one step in a Thermolyne 46100 furnace (Barnstead, Dubuque, IA).[13] Cannillo showed that powdered glass infiltration creates significantly better infiltration than bulk glass infiltration.[22]

To investigate the effect of infiltrating duration on the flexural load, specimens were divided into 3 groups of 6 and infiltrated at 1550 °C for 1 h, 2 h, and 3 h respectively. A heating and cooling rate of 500 °C per hour were utilized. The selected infiltrating temperature was below the sintering temperature of alumina, to avoid significant grain growth. An additional group of 6 was left untreated to serve as the control. The glass infiltrated specimens were abraded with a 3 μm diamond disk to remove residual surface glass and then polished with a 0.5 μm disk to ensure that total specimen thickness remained at 1.5 mm and to produce a surface finish similar to the uninfiltrated alumina plates in the control group.

20 additional glass infiltrated specimens were created at the 2 h time point after it showed the highest flexural load resistance. Specimens were subjected to dynamic fatigue testing as detailed below.

2.2. Materials characterization

Selective specimens (at least three specimens from each testing group) were subjected to scanning electron microscopy (SEM), X-ray diffractometry (XRD) and microindentation analyses.

2.2.1. SEM analysis

Specimens were sectioned along the modulus gradients using a water cooled low speed diamond saw (Isomet, Buehler, Lake Bluff, IL). The cross-sections were polished to 0.5 μm finish and subjected to thermal etching at 1500 °C for 20 min with a heating and cooling rate of 500 °C per hour. The polished and etched sections were carbon coated prior to SEM examination (Hitachi 3500N, Japan).

2.2.2. X-ray diffractometry

To determine the crystallinity of the external surface residual glass and the graded layers, as infiltrated glass–alumina graded surface (with an external glass layer) were subjected to XRD (Philips X'Pert System, Almelo, Overijssel, Netherlands) analysis with nickel filtered Cu K_α radiation. XRD data was taking from 5° to 80° at 45 kV and 45 mA at a scanning rate of 1°/min and a step size of 0.02°. Spectrum was analyzed for homogenous alumina, the graded layer, and the external glass to show the amorphous glass phase expected on the surface and to ensure that no phase change occurs within the alumina and that no additional crystal phase is formed on the surface upon cooling from the glass infiltration temperature.

2.2.3. Micro-indentation

Micro-indentation was performed on a 3D Omniprobe TriboIndenter (Hysitron, Minneapolis, MN) to measure the hardness and elastic modulus as they change in relationship with depth. Indentation provides measurements of elastic modulus and hardness over a small surface, allowing for specific readings at increments of the glass–ceramic gradient. Specimens ($n = 3$) from each infiltration duration (i.e. 1, 2, and 3 h)

were embedded in a resin epoxy and sectioned and polished to 0.5 μm finish. Measurements were taken along the graded cross section with a Berkovich indenter at 50 mN with a step size of 10 or 20 μm. The reduced modulus was determined by the Oliver-Pharr approach[23] from the indentation curve. The Young's modulus of the specimen was computed using the measured reduced modulus. The reduced modulus, E_r, is described by the relationship:

$$\frac{1}{E_r} = \frac{1-{v_i}^2}{E_i} + \frac{1-{v_s}^2}{E_s} \quad (1)$$

where E and ν are the Young's modulus and Poisson's ratio of the indenter (i) or tested sample (s), respectively. For a diamond indenter tip, E_i is 1140 GPa and ν_i is 0.07. For alumina, glass, and graded alumina–glass materials, ν_s is 0.22.

2.3. Indentation flexural testing

The specimens were bonded to the surface of a compliant substrate of polycarbonate (Sheffield Plastics, Sheffield, MA) using a fast setting epoxy (Hardman Red, Royal Adhesives and Sealants, Belleville, NJ).[24] Here we adopted a ball-on-ceramic/polymer bilayer method to determine the critical fracture load of a bending plate (Fig. 1).[1,4,25] The ball-on-flat bilayer indentation flexural test produces bending stresses in the ceramic layer just like those generated by a biaxial or three-point bend test, and yet is more tolerant to the specimen dimensions, capable of testing specimens with smaller thicknesses and irregular shapes. In addition, this ceramic/polymer bilayer system represents the ceramic crown on dentin structure and thus, upon indentation fracture, produces clinically relevant failure modes.[4,26]

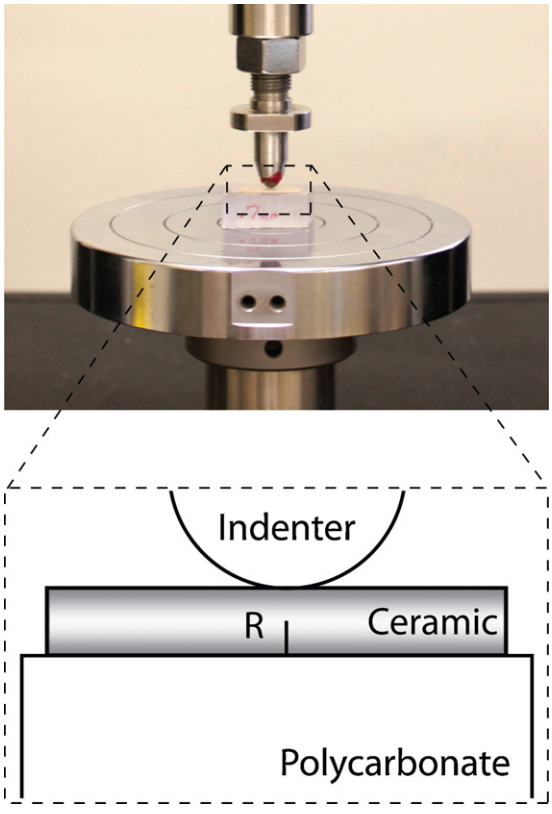

Fig. 1. (a) Indentation loading rig with specimen bonded to polycarbonate substrate and (b) schematic of test geometry showing radial crack (R) initiating from the lower surface of ceramic specimen.

The specimens were loaded into an universal testing machine (Instron 5566, Norwood, MA) (Fig. 1). A spherical tungsten carbide indenter ($r = 3.18$ mm) was used as the contactor (see insert of Fig. 1). Specimens were loaded monotonically at a rate of 1 mm/min. Failure was defined by the onset of flexural radial cracks (R) at the ceramic lower surface (see insert of Fig. 1). Critical load corresponding to the radial crack pop-in was determined by a machine noted load drop. Continuous data points were recorded during the test for load and extension, as well as load and extension at the point of failure.

The slow crack specimens were loaded similarly at progressively decreasing rates to investigate SCG. Tests included rates in decades between 1 and 10^{-4} mm/min ($n = 5$, each rate). Test rates (mm/min) were converted to N/s for each data point. The specimen was loaded at a fixed rate $\mathrm{d}F/\mathrm{d}t = $ constant until initiation of a radial crack at a critical load F_R

$$F_R = \frac{\mathrm{d}F}{\mathrm{d}t} t_R \quad (2)$$

where t_R is the elapsed time to produce the radial crack.

Previous studies showed that the velocity exponent N that describes the SCG behavior of the material can be determined with the equation below.[3]

$$\frac{F_R}{d^2} = \left[\frac{A'(N+1)\dot{F}}{d^2}\right]^{1/(N+1)} \quad (3)$$

where A' is a load-, time-, and thickness-independent quantity,[27] F_R is the ultimate load (N), $\dot{F} = \mathrm{d}F/\mathrm{d}t$ is the load rate (N/s), and d is the plate thickness (mm).

Therefore, by plotting the $F_R - \dot{F}$ curve in logarithmic coordinates, the N value can be readily derived from the slope of best-fit curves.

Substituting Eq. (2) into Eq. (3), we obtain the F_R–t_R relation for dynamic fatigue:

$$\frac{F_R}{F_0} = \left(\frac{t_0}{t_R}\right)^{1/N} \quad (4)$$

where F_0 and t_0 are reference parameters relating to short-term tests.

Finally, by using Eq. (4) and experimentally determined N and t_R values, fracture load corresponding to various load rates can be collapsed to short-term fracture load, which can be related to the inert ceramic strength, σ_0, using equation[3]:

$$\sigma_0 = B\left(\frac{F}{d^2}\right) \quad (5)$$

where $B = 0.75\log(E_c/E_s)$. E_c and E_s are elastic modulus for ceramic and substrate respectively. This provided a pool of short-term fracture load data of graded and homogenous alumina for Weibull statistical analysis.

2.4. Weibull modulus m

To provide reliable prediction of fracture resistance of ceramics, the Weibull failure probabilities should be taken into account. The Weibull failure probability is described by the Weibull modulus, m. A higher m value indicates a smaller scatter in measured properties.

In terms of critical load F_m of brittle layers, the Weibull failure probability P can be defined as

$$P = 1 - \exp\left[-\left(\frac{F_m}{F_0}\right)^m\right] \quad (6)$$

where F_0 is a scaling load. For a data set of critical loads, cumulative probabilities are calculated by ranking values in ascending order and evaluating corresponding F values. A plot of $\ln(\ln(1/(1-P)))$ against $\ln F_m$ gives a straight line with slope m.

3. Results

Representative SEM micrographs of graded glass–alumina surface (top) and pure alumina interior core (bottom) are shown in Fig. 2. In this case the specimen was glass infiltrated at 1550 °C for 2 h. However, detailed examinations on specimens infiltrated at 1, 2, or 3 h revealed similar microstructural features. The glass content at the graded glass–alumina surface was relatively high, which decreased as the distance from the surface increased. Eventually the graded glass–alumina layer gave way to a highly crystalline alumina core.

The gradation of Young's modulus along the depth (from both top and bottom surfaces to interior) of graded alumina infiltrated at 1, 2, or 3 h is shown in Fig. 3. Data revealed a relatively low Young's modulus at the hybrid glass–alumina

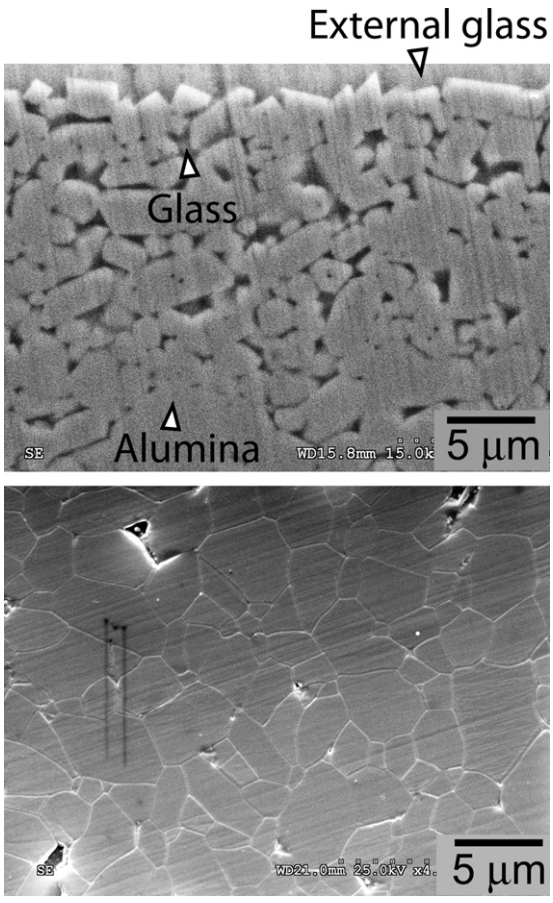

Fig. 2. Graded specimen showing infiltrated glass surface and graded glass–alumina layers (top) and dense alumina core (bottom) after thermal etch.

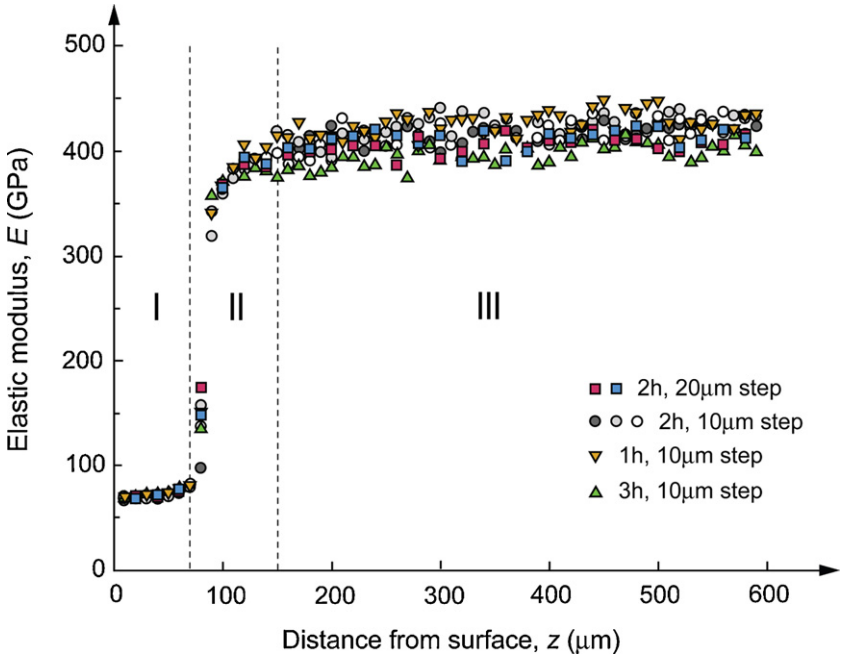

Fig. 3. Indentation profile of glass infiltrated alumina. (I) External glass layer, (II) graded glass–alumina transition region, and (III) dense alumina core.

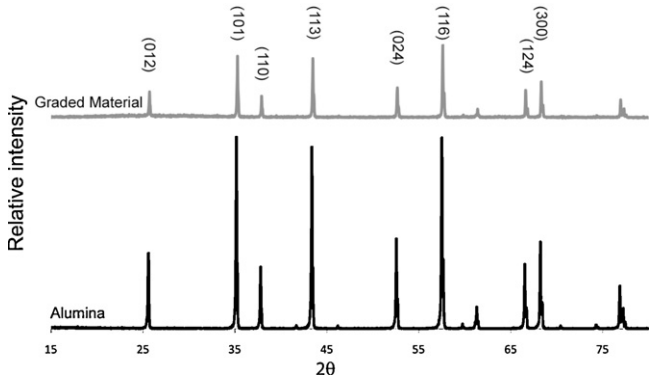

Fig. 4. XRD comparison of graded (top) and control (bottom) specimens. Major peaks for α-alumina are indexed. No new crystalline phases are noted after infiltration as compared to the control specimen. Amorphous glass is visible as low hump near the first alumina peak.

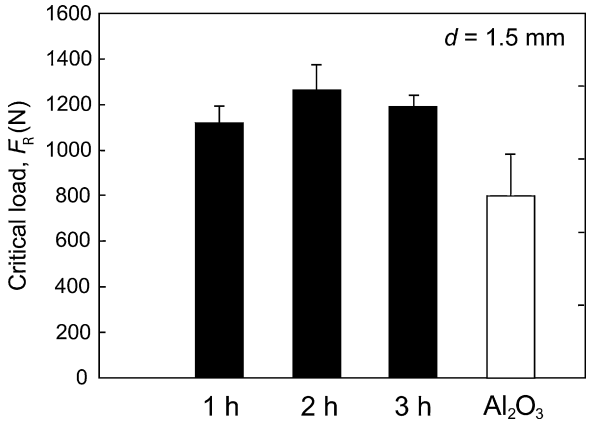

Fig. 5. Fast loading (1 mm/min) experiments with specimens treated for 1, 2, and 3 h and untreated control. Significant increase in load-bearing capacity was seen between all treated specimens and control. No significant difference was found between the 3 treated groups.

surface, which rose rather quickly to the bulk modulus of alumina as the distance from the surface increased. The residual glass layer ($d \approx 60$–$70\,\mu m$, labeled as zone I in Fig. 3) possessed a Young's modulus value of $E = 68.3 \pm 2.5$ GPa (mean ± S.D., $n = 85$). For the glass–alumina graded layer ($d \approx 80\,\mu m$, marked as zone II), the Young's modulus varied from $E = 109.7 \pm 5.9$ GPa ($n = 10$) near the external glass/graded layer interface to $E = 418.9 \pm 17.4$ GPa ($n = 510$) at the alumina interior (identified as zone III). Note that the n values quoted in parentheses, $n = 85$, 10, and 510, represent number of indents made in the external glass layer, graded layer surface, and the alumina interior, respectively, from a total of 12 specimens.

One concern of the graded glass–alumina structures was the crystallization of glass during cooling from the infiltration temperature, both in the external surface glass layer and in the graded glass–alumina layer. Changes in glass composition and structure could alter its CTE and thus introduce residual stresses to the graded material. XRD analysis of the as infiltrated glass–alumina surfaces revealed a small amount of glass phase in the external glass and graded glass–alumina layers (Fig. 4). There was no detectable secondary crystalline phase present in addition to the α-alumina phase, at least within the detection limit of XRD (i.e. ~3 vol.%). For reference, an XRD spectrum of a sintered homogenous alumina, prior to glass infiltration, is shown in Fig. 4. In addition, energy dispersive X-ray (EDX) analysis confirmed identical compositions in uninfiltrated and infiltrated glasses, indicating no essential change in properties during infiltration.

Critical load for fast loading (1 mm/min) flexure-induced fracture of graded glass–alumina infiltrated at various dwell time periods is shown in Fig. 5. Although a trend may be noted which hints at a higher fracture load in the 2 h samples, this trend was not statistically significant. However, all three groups showed improved fracture resistance over untreated alumina, indicating that the induced gradient does produce the desired effect. The 2 h treatment time was chosen for continued dynamic fatigue samples.

Results of the dynamic fatigue tests are shown as F_R/d^2 versus $\dot{F}/d^2$ in logarithmic coordinates in Fig. 6. Normalization of F_R to d^2 enables direct comparison of critical loads for ceramic layers of different thicknesses, effectively reducing all data to one nominal thickness. Solid lines are best fit regressions for each data set, while shaded bands are 95% confidence bounds. Data showed the expected rate dependence; critical load decreased as load rate decreased. The graded glass–alumina composite retained higher load bearing capacity at all tested rates, despite also following a higher rate dependence than alumina controls. SCG exponents, N, were derived from the inverse slopes of the fitted lines. $N = 17$ for graded glass–alumina and $N = 27$ for alumina. The N value for alumina is similar to that obtained in a previous study ($N = 26$)[3] using the same alumina plates but different thicknesses bonded onto polycarbonate substrates, confirming the reproducibility of the current test methods.

Weibull plots for nominal critical load data on graded and homogenous alumina plates are shown in Fig. 7. Critical load data corresponding to different load-rates were reduced to nominal F_m for plates of 1.5 mm thickness using a common load rate 100 N/s. Linear regression fit (shown as solid lines) seemed

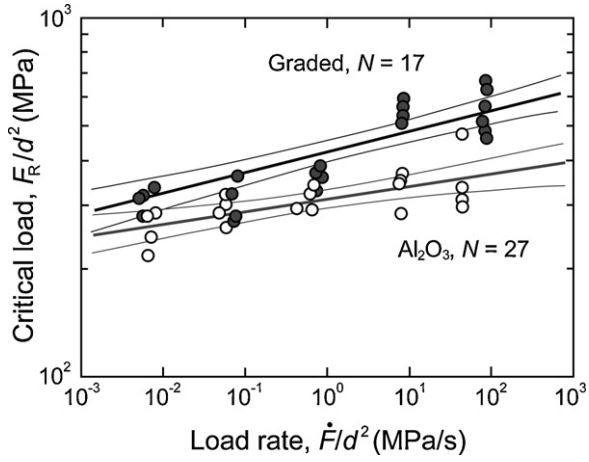

Fig. 6. Critical load versus load rate normalized against specimen thickness (d^2). Linear regression and 95% confidence bounds shown for both graded (top) and alumina (bottom) specimens.

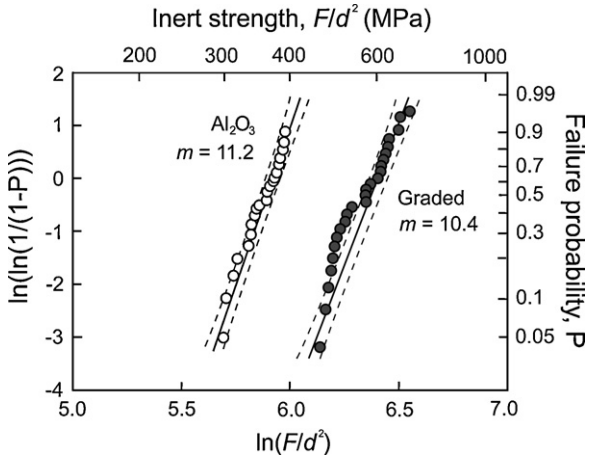

Fig. 7. Weibull plot including slow crack growth data collapsed to a nominal 100 N/s and normalized against specimen thickness (d^2). Linear regression (solid lines) and 95% confidence bounds (dashed lines) shown for both graded (right) and alumina (left) specimens.

to be reasonable representations of the data for both materials; Weibull moduli m were derived from the slope of the linear lines. In our Weibull analysis, we used the nominal critical load instead of flexural strength for graded alumina. Although the flexural strength is proportional to nominal critical load ($\sigma \propto F_m/d^2$, Eq. (5)), flexural strength for graded alumina may not be readily derived owing to the variations of the stress profile in the graded region. Our analysis showed that graded alumina exhibited similar Weibull modulus ($m = 10.4$) compared to homogeneous alumina ($m = 11.2$). However, alumina with elastic grading at the flexural surface showed significantly higher load-bearing capacity than their homogeneous counterparts.

4. Discussion

The initial, fast loading experiments showed a very clear increase in load-bearing capacity in graded alumina over its homogenous counterpart by a factor of approximately 1.5 (Fig. 5). A one tailed t-test produces a p-value smaller than $\alpha = 0.025$, indicating that the difference between the graded material with a 2 h treatment and the mean for alumina controls is significant. However, little difference was seen in critical load for samples infiltrated for various durations (1, 2, and 3 h). The increase in load-bearing capacity can be explained by a change in the flexural tensile stress profile in the graded material under load, as suggested by Zhang and Kim.[13] Composite beam theory[14] and finite element analysis[12] show that a lower-modulus surface graded layer can effectively reduce the surface stress and transfer the maximum stress to the ceramic interior, improving the load-bearing capacity.

As previously explained, the bottom surface of a homogeneous specimen under flexural load will be experiencing the highest tensile stress in the material. This is the point where flexural radial crack will initiate, due to the susceptibility of ceramics to tensile stress. If the stress at this point is lowered, we will see a lower likelihood of critical crack propagation beginning at surface flaws. Further, if the peak stress is pushed away from the material surface, internal flaws will bear this maximum. The absence of large internal flaws, coupled with the somewhat diminished effectiveness of any such internal flaws as stress concentrators,[28] renders the graded material more flaw tolerant. The increased stress tolerance of graded materials relative to homogenous materials explains the higher critical loads for flexural radial fracture observed experimentally. Thus, the load-bearing capacity of the ceramic material is significantly improved by reducing the surface tensile stress and shifting the maximum stress into the interior.

Our experimental data also showed a similar load-bearing capacity for graded alumina infiltrated for various durations (Fig. 5). Micro-indentation tests revealed almost no difference in Young's modulus gradients amongst these specimens (Fig. 2), suggesting that effects of surface elastic gradients on load-bearing capacity in these graded materials should also be similar. The lack of dependence of infiltration depth on infiltration time and a fairly steep grading observed in all specimens are probably due to the relatively low infiltration temperature (1550 °C) utilized in this study. Jitcharoen and co-workers infiltrated fully sintered alumina using an aluminosilicate glass at 1690 °C for 2 h, the resultant infiltration depth was ~2 mm.[10] However, the trade-off for using such a high infiltration temperature is the grain growth of alumina particles and crystallization of the infiltrating glass, which in turn would compromise the flexural strength and the aesthetic appearance of graded aluminas. The effect of graded to total layer thickness ratio on the strength of these graded structures has been examined analytically[14] and experimentally[12] in several previous publications.

Question then arises as to whether the increased load-bearing resistance in graded alumina relative to their monolithic counterparts is due to the residual stresses introduced to the graded materials upon cooling. This residual stress can form from the crystallization and/or compositional changes of the infiltrating glass, which in turn could modify the CTE of glass. A compressive residual stress at the surface can also improve the flexural damage resistance. Our XRD analysis of the as infiltrated glass–alumina surfaces revealed a predominant α-alumina phase with a broad amorphous glass peak (Fig. 4). There was no detectable secondary crystalline phase present. In addition, EDX analysis revealed no essential compositional changes in glass before and after infiltration. SEM and optical microscopies revealed a highly transparent appearance of the external glass. Thus, our findings suggest that there are no significant residual stresses induced through microstructural changes during the glass infiltration process.

The dynamic fatigue loading experiments also show an improved flexural resistance in graded alumina. In this experiment, there was less surety of a favorable outcome. This is borne out by the lower N exponent in the graded materials, an indicator of higher load rate dependence on crack growth (Fig. 6). It was theorized that the load-bearing capacity of the graded material would eventually be lower than that of the homogeneous control. The estimated critical point where the control shows

better flexural resistance than the graded material would be over 3 years. This is because cracks would propagate faster in the glass phase, which is more susceptible to moisture-assisted SCG. Thus the slower rate of dynamic tests would increase susceptibility of crack growth in the glass-rich regions.

In clinical applications, these graded alumina materials can be used as monolithic crowns and bridges. Although the graded alumina has limited translucency, the external glass layer and the graded glass–alumina layer provide necessary shade options. In addition, color stains can be applied to the surface of the external glass layer using a powdered glass slurry that has similar composition to the infiltrated glass. This staining technique has been used on the Empress system to improve the aesthetic outcome of a single color pressed block of glass ceramic and is well established in aesthetic dentistry.[29,30] To improve aesthetics, a thin porcelain veneer with similar compositions to the infiltrated glass can be applied to the surface of the external glass layer. This thin veneer could contain the contact damage, provide aesthetics, prevent excessive wear of opposing dentition, and allow for adjustment on the occlusal surface. Any occlusal-surface contact damage can be confined within the thin veneer layer, because cracks are unlikely to propagate from a low modulus, low toughness porcelain to a higher modulus, higher toughness alumina.[31]

The external glass and the graded glass–alumina layers on the cementation surface (the tensile surface) of graded aluminas offer great potential for adhesive bonding using etching-silane techniques. The external glass layer and the glass phase in the graded layer can be selectively removed by hydrofluoric acid, creating a three-dimensional surface morphology and enhancing physical adhesion. A strong resin bond can be achieved through the application of a silane coupling agent.

5. Conclusions

The observed behavior was significant as an indicator of the interaction between the modulus gradients and stress distributions. Our findings have demonstrated that significantly improvement in load bearing capacity of ceramics can be achieved by appropriate elastic grading at the surface. The observed behavior was due to a reduction of the surface stress and to a shift of the maximum tensile stress into the depth of the material. It was also shown that the resulting increased susceptibility to SCG did not limit material strength or reliability below that of homogenous alumina for the load rate tested.

Acknowledgements

Valuable discussions with Prof. Van P. Thompson and Dr. Brian R. Lawn are appreciated. Thanks are due to Drs. Sanjit Bhomwick and Yvonne Gerbig for conducting nanoindentation measurements, and Dr. Hong Zhao for performing XRF analysis. This investigation was supported in part by Research Grant CMMI-0758530 (PI. Zhang) from the US Division of Civil, Mechanical & Manufacturing Innovation, National Science Foundation and Research Grant R01 DE017925 (PI. Zhang) from the US National Institute of Dental & Craniofacial Research, National Institutes of Health.

References

1. Lawn BR, Deng Y, Thompson VP. Use of contact testing in the characterization and design of all-ceramic crownlike layer structures: a review. *J Prosthet Dent* 2001;**86**:495–510.
2. Studart AR, Filser F, Kocher P, Gauckler LJ. In vitro lifetime of dental ceramics under cyclic loading in water. *Biomaterials* 2007;**28**:2695–705.
3. Zhang Y, Lawn B. Long-term strength of ceramics for biomedical applications. *J Biomed Mater Res B: Appl Biomater* 2004;**69**:166–72.
4. Lawn BR, Deng Y, Miranda P, Pajares A, Chai H, Kim DK. Overview: damage in brittle layer structures from concentrated loads. *J Mater Res* 2002;**17**:3019–36.
5. Huang M, Wang R, Thompson V, Rekow D, Soboyejo WO. Bioinspired design of dental multilayers. *J Mater Sci Mater Med* 2007;**18**:57–64.
6. Taskonak B, Mecholsky JJ, Anusavice Jr KJ. Residual stresses in bilayer dental ceramics. *Biomaterials* 2005;**26**:3235–41.
7. Aboushelib MN, Feilzer AJ, de Jager N, Kleverlaan CJ. Prestresses in bilayered all-ceramic restorations. *J Biomed Mater Res B: Appl Biomater* 2008;**87**:139–45.
8. Erdogan F. Fracture-Mechanics of Functionally Graded Materials. *Compos Eng* 1995;**5**:753–70.
9. Tesch W, Eidelman N, Roschger P, Goldenberg F, Klaushofer K, Fratzl P. Graded microstructure and mechanical properties of human crown dentin. *Calcif Tissue Int* 2001;**69**:147–57.
10. Jitcharoen J, Padture NP, Giannakopoulos AE, Suresh S. Hertzian-crack suppression in ceramics with elastic-modulus-graded surfaces. *J Am Ceram Soc* 1998;**81**:2301–8.
11. Suresh S. Graded materials for resistance to contact deformation and damage. *Science* 2001;**292**:2447–51.
12. Zhang Y, Chai H, Lawn BR. Graded structures for all-ceramic restorations. *J Dent Res* 2010;**89**:417–21.
13. Zhang Y, Kim JW. Graded structures for damage resistant and aesthetic all-ceramic restorations. *Dent Mater* 2009;**25**:781–90.
14. Zhang Y, Ma L. Optimization of ceramic strength using elastic gradients. *Acta Mater* 2009;**57**:2721–9.
15. Chevalier J. What future for zirconia as a biomaterials? *Biomaterials* 2006;**27**:534–43.
16. Chevalier J, Cales B, Drouin JM. Low-temperature aging of Y-YZP ceramics. *J Am Ceram Soc* 1999;**82**:2150–4.
17. Chevalier J, Gremillard L. Ceramics for medical applications: a picture for the next 20 years. *J Eur Ceram Soc* 2009;**29**:1245–55.
18. Hirano M. Inhibition of low-temperature degradation of tetragonal zirconia ceramics—a review. *Br Ceram Trans J* 1992;**91**:139–47.
19. Piconi C, Maccauro G. Zirconia as a ceramic biomaterial. *Biomaterials* 1999;**20**:1–25.
20. Kim JW, Covel NS, Guess PC, Rekow ED, Zhang Y. Concerns of hydrothermal degradation in CAD/CAM zirconia. *J Dent Res* 2010;**89**:91–5.
21. Standard Test Methods for Determining Average Grain Size. E 112-96ϵ_2. ASTM International, 100 Barr Harbor Drive, PO Box C700, West Conshohocken, PA 19428-2959, United States; 2003.
22. Cannillo V, Lusvarghi L, Manfredini T, Montorsi M, Siligardi C, Sola A. Glass-ceramic functionally graded materials produced with different methods. *J Eur Ceram Soc* 2007;**27**:1293–8.
23. Oliver WC, Pharr GM. An improved technique for determining hardness and elastic-modulus using load and displacement sensing indentation experiments. *J Mater Res* 1992;**7**:1564–83.
24. Deng Y, Lawn BR, Lloyd IK. Characterization of damage modes in dental ceramic bilayer structures. *J Biomed Mater Res* 2002;**63**:137–45.
25. Lawn BR. Ceramic-based layer structures for biomechanical applications. *Curr Opin Solid State Mater Sci* 2002;**6**:229–35.

26. Lawn BR, Pajares A, Zhang Y, Deng Y, Polack MA, Lloyd IK, et al. Materials design in the performance of all-ceramic crowns. *Biomaterials* 2004;**25**:2885–92.
27. Lee CS, Kim DK, Sanchez J, Miranda P, Pajares A, Lawn BR. Rate effects in critical loads for radial cracking in ceramic coatings. *J Am Ceram Soc* 2002;**85**:2019–24.
28. Lawn BR. *Fracture of brittle solids*. Cambridge: Cambridge University Press; 1993.
29. Dong JK, Luthy H, Wohlwend A, Scharer P. Heat-pressed ceramics: technology and strength. *Int J Prosthodont* 1992;**5**:9–16.
30. Luthy H, Dong JK, Wohlwend A, Scharer P. Effects of veneering and glazing on the strength of heat-pressed ceramics. *Schweiz Monatsschr Zahnmed* 1993;**103**:1257–60.
31. Kim JW, Bhowmick S, Hermann I, Lawn BR. Transverse fracture of brittle bilayers: relevance to failure of all-ceramic dental crowns. *J Biomed Mater Res B: Appl Biomater* 2006;**79**:58–65.